11th World Congress on Computational Mechanics (WCCM XI)
5th European Conference on Computational Mechanics (ECCM V)
6th European Conference on Computational Fluid Dynamics (ECFD VI)
E. Oñate, J. Oliver and A. Huerta (Eds)

ON THE DEVELOPMENT OF A HARMONIC BALANCE METHOD FOR AEROELASTIC ANALYSIS

Graham Ashcroft, Christian Frey, Hans-Peter Kersken*

German Aerospace Center (DLR)
Institute of Propulsion Technology
Linder Höhe, 51147 Cologne, Germany
email: graham.ashcroft@dlr.de, christian.frey@dlr.de, hans-peter.kersken@dlr.de

Key words: Harmonic Balance Method, Flutter, Aeroelasticity, Turbomachinery

Abstract. To efficiently simulate time-periodic, non-linear flows in turbomachinery a Harmonic Balance (HB) method has recently been developed within the framework of DLR's compressible, Unsteady Reynolds Averaged Navier-Stokes (URANS) solver TRACE. As a hybrid time- and frequency-domain method, that solves directly for the complex valued solution harmonics of the URANS equations, the approach allows both the integration of highly accurate non-reflecting boundary conditions and the efficient resolution of non-linear flow phenomena. In the current work the HB-solver is extended and applied to investigate the aeroelastic problem of flutter in turbomachinery. Within this context the HB-method is developed, under consideration of the Geometric Conservation Law (GCL), to support deforming meshes. To validate the approach the well documented aeroelastic test case Standard Configuration 10 is simulated and results are compared to those obtained with an inhouse time-linearized solver and reference data from the literature.

1 INTRODUCTION

Aeroelastic analysis is an integral aspect of the design of compressor and turbine components. To investigate such complex phenomena efficient numerical methods capable of accurately capturing the underlying unsteady interaction between the blades and aerodynamic flow field are required. As the physical phenomena of flutter and forced-response are periodic in nature the associated numerical simulations are typically formulated in the frequency domain. Due to limited computation resources the earliest work on frequency domain solvers for aeroelasticity investigations was based on the two-dimensional Euler equations [7]. With the advent of ever more powerful computer resources the underlying models have been extended to the three-dimensional Euler equations and more recently to the three-dimensional compressible Navier-Stokes equations.

To facilitate the transformation of the governing equations to the frequency domain all of these approach are based on the linearization of the governing equations. This decouples the governing equations for the flow perturbations from those governing the mean flow field and enables highly efficient solvers to be developed. Whilst highly efficient this approach negates the application of such tools to problems in which nonlinear phenomena are suspected to play an imporant role.

To overcome these restrictions and allow frequency-domain methods to be applied to nonlinear, time-periodic problems considerable effort has been expended in recent years in the development of harmonic balance (HB) methods.

In this work the Harmonic Balance method implemented in the CFD solver TRACE [4] is extended to investigate the problems of flutter and forced-response in turbomachinery. The paper is organised as follows. In Section 2 the basic numerical approach is outlined in terms of the underlying CFD solver and the basic Harmonic Balance method. The extension of the HB-solver to support deforming meshes is then described in Section 2.2.2. The validation of the HB-solver for deforming meshes is then presented in Section 3 using a simple channel flow with a deforming mesh. In Section 4 the HB-method is then applied to the benchmark aeroelasticity problem Standard Configuration 10 and the ability of the approach to capture nonlinear effects in the unsteady flow is investigated. Finally, in Section 5 a summary of the conclusions of the work is given.

2 NUMERICAL METHOD

2.1 Underlying Flow Solver

The harmonic balance method described in this work is part of the CFD code TRACE. TRACE [1] is a parallel Navier-Stokes flow solver for structured and unstructured grids that has been developed at DLR's Institute of Propulsion Technology in Cologne to model and investigate turbomachinery flows. The code solves the finite-volume discretization of the compressible Reynolds-averaged Navier-Stokes (RANS) equations in the relative frame of reference using a multi-block approach. Inviscid fluxes are evaluated using Roe's flux-differencing-splitting method. The upwind states are computed using the MUSCL family of schemes in conjuction with a modified van Albada limiter to avoid unphysical oscillations in the vicinity of shocks. Viscous terms are discretized using second-order accurate central differences. To model the effects of turbulence various turbulence and transition models have been integrated in the code [2]. For the present work it is sufficient to note that following the discretization of the spatial operators in the Navier-Stokes equations the following system of ordinary differential equations (ODEs) is obtained

$$\frac{dq}{dt} + R\left(q(t)\right) = 0 \tag{1}$$

where q is the vector of conservative variables, R is the discretized RANS residual vector and t denotes the physical time.

2.2 Harmonic Balance Method

In the current work we are interested in time-periodic solutions of Eq. 1. Often such problems can be accurately described by a limited number of solution harmonics, e.g.

$$q(x,t) = \mathrm{Re}\left[\sum_{k=0}^{K} \hat{q}_k(x) e^{ik\omega t}\right] \tag{2}$$

where $\hat{q}_k$ are the complex valued solution harmonics and $\omega = 2\pi f$ is the fundamental angular frequency. In such cases it is attractive to formulate the unsteady problem, Eq. 1, in the frequency domain, i.e. to consider

$$\mathbf{i}k\omega\hat{q}_k + \widehat{R(q)}_k = 0, \tag{3}$$

for only a finite number of harmonics, $k = 0, \ldots, K$. For configurations in which nonlinearity can be assumed to be negligble the coupling between the harmonics of q, imposed by the nonlinear nature of R, can be neglected and one obtains $K+1$ independent equations for the solution harmonics and the time-mean solution field. However, if one wishes to retain nonlinear effects an alternative approach is required in the modelling or computation of $\widehat{R(q)}_k$. In this work we compute $\widehat{R(q)}_k$ as $\mathscr{F}(R(\mathscr{F}^{-1}\hat{q}))|_k$ and therefore solve

$$\mathbf{i}k\omega\hat{q}_k + \mathscr{F}(R(\mathscr{F}^{-1}\hat{q}))|_k = 0, \tag{4}$$

where $\mathscr{F}$ denotes the Discrete Fourier Transform (DFT).

Eqn. 4 is solved directly in the frequency domain to obtain the complex valued harmonics of the conservative variables $\hat{q}_k$. To compute the harmonics of the RANS residual vector R the solution field vector is first reconstructed at N sampling points within the period of oscillation from the Fourier coefficients of the conservative variables $\hat{q}_k$ using an inverse DFT. Using the reconstructed solution vectors the RANS residual vectors R are then computed at the N sampling points to enable the DFT of R to be computed. Note, since the RANS residual R is evaluated in the time-domain the standard flux and discretization schemes from the underlying nonlinear solver can be used without the need to explicitly model the coupling terms between the solution harmonics.

As a hybrid time- and frequency-domain method the approach has the advantage, over methods formulated purely in the time- or frequency-domain, of being able to employ not only the possibly highly nonlinear time-domain flux functions (and their stabilizing numerical limiters) but also highly accurate nonreflecting boundary conditions formulated in the frequency domain [5]. Particularly in the context of aeroelasticity or aeroacoustics should boundary conditions are of the utmost importance.

2.2.1 Harmonic Sets

The application and solution of Eqn. 4 is straightforward if the problem at hand can be described by harmonics of a single fundamental frequency. On the otherhand, if multiple

fundamental frequencies are present, e.g. blade row interaction in a multistage compressor or turbine, the application of Eqn. 4 is more involved. If the fundamental frequencies do not share a common base frequency the DFT used in Eqn. 4 is essentially approximative and great care must be taken in selecting the sampling times and sample duration if the accuracy and stability of the approach is to be significantly reduced [6]. In certain cases the fundamental frequencies may be integer multiples (harmonics) of a common third fundamental frequency. However, if the difference in frequency between the original two fundamental frequencies Δf is small then the common fundamental frequency will be equally low ($f = \Delta f$) and the harmonics of interest high. This reduces the efficiency of the approach significantly as the number of sampling points required is proportional to the order of the harmonics to be resolved.

To overcome these difficulties the concept of *harmonic sets* $\mathscr{S}_i$ is introduced [4]. A harmonic set is defined by a fundamental angular frequency (ω) and interblade phase angle (σ), fundamental mode, and higher harmonics, e.g.

$$\mathscr{S} = \{(k_1\omega, k_1\sigma), (k_2\omega, k_2\sigma), \ldots\}\,. \tag{5}$$

For each fundamental mode a harmonic set is defined. As a given mode may exist simultaneously in multiple harmonic sets, e.g. the zeroth harmonic or time-mean solution, the harmonic sets can not be treated entirely independently without the duplicate modes being ill-specified. To address this deficiency the RANS residual is extended to couple the harmonic sets via the duplicate modes and approximated (in the case of two harmonic sets) by

$$R(q_{\mathscr{S}_1\cup\mathscr{S}_2}(t)) \approx R(q_{\mathscr{S}_1}(t)) + R(q_{\mathscr{S}_2}(t)) - R(q_{\mathscr{S}_1\cap\mathscr{S}_2}(t)), \tag{6}$$

allowing the harmonics of the residual to be computed as the sum of the harmonics of the residuals on the right-hand side of Eqn. (6). The main advantage of this approach is that the sampling points for each of the harmonic sets $\mathscr{S}_1$, $\mathscr{S}_2$ and $\mathscr{S}_1 \cap \mathscr{S}_2$ can be chosen independently. Applying the specific DFT to each of the three summands then yields the harmonics of the residual. For more details see [4].

2.2.2 Time-dependent Meshes

To simulate the problem of flutter it is necessary to be able accomodate time-dependent boundaries and therfore meshes. For such problems the RANS residual depends not only on the time-dependent solution vector q but also on the grid coordinates x and the grid velocities $\dot{x}$, i.e.

$$R = R(q, x, \dot{x}). \tag{7}$$

Furthermore, in constrast to Eqn. 1 the cell volume is time-dependent and must be retained in the temporal derivative term. The governing equations then read

$$\frac{\partial}{\partial t}\left(Vq\right) + R\left(q(t), x(t), \dot{x}(t)\right) = 0 \tag{8}$$

where V is the, time-dependent, volume of a given cell. Since for flutter problems the blade surface motion is time-periodic the mesh displacement can be discribed by

$$\delta x(x,t) = \mathrm{Re}\left[\hat{x}(x)e^{i\omega t}\right] \tag{9}$$

where $\hat{x}$ is the complex valued displacement vector. Using Eqn. 9 the HB-solver can be extended for periodically deforming meshes by reconstructing the mesh alongside the flow field at the N sampling points. Furthermore, Eqn. 9 is used to compute the grid velocities $\dot{x}$. With the mesh geometry at the N sampling points known all required metrics as well as the Jacobian $J = 1/V$ can be calculated and used in the evaluation of the RANS residual R and the computation of its harmonics.

In contrast to the situation with stationary meshes care must also be taken when evaluating the temporal harmonic of the temporal derivative term in Eqn. 8. For stationary meshes this is simply $\mathbf{i}k\omega\frac{\hat{q}_k}{J}$. However for deforming meshes we require

$$\mathbf{i}k\omega\widehat{\left(\frac{q}{J}\right)\Big|}_k. \tag{10}$$

That is, the harmonics of the volume weighted conservative flow variables are required. As we solve for the harmonics of the conservative flow variables these data are not directly available. One approximate, but computationally efficient, approach to compute the term in Eqn. 10 is to employ its linearized form and compute

$$\mathbf{i}k\omega\hat{q}_k\frac{J - J_0}{J_0^2}, \tag{11}$$

where J_0 is the Jacobian of the undisturbed mesh. This is the approach adopted in the linear solver linearTRACE [8]. Whilst suitable for small amplitude mesh displacement, and therefore a linear solver, the approach was found to produce large amplitude spurious pressure waves at large amplitudes. To overcome this limitation the time-derivative term is computed by computing directly the harmonics of the weighted conservative flow variables from the reconstructed mesh and flow time-histories. Although somewhat more computationally expensive this approach ensures the time-dependent mesh displacement does not corrupt the solution at large amplitude disturbances.

2.2.3 Solution Techniques

To solve the governing equations an implicit pseudo-time approach is adopted. Discretizing the pseudo-time operator using the first-order Euler backward method and then linearizing the harmonic balance residual R^{HB} in pseudo-time the following system of equations is obtained

$$\left[\frac{1}{J_0}\left(\frac{1}{\Delta\tau}+\mathbf{i}k\omega\right)+\left.\frac{\partial R}{\partial q}\right|_{\hat{q}_0^{(m)}}\right]\Delta\hat{q}^{(m)}=-R_k^{\mathrm{HB}}\left(\hat{q}^{(m)}\right), \tag{12}$$

where

$$R_k^{\mathrm{HB}}\left(\hat{q}^{(m)}\right)=\mathbf{i}k\omega\left.\widehat{\left(\frac{q}{J}\right)}\right|_k+\mathscr{F}(R(\mathscr{F}^{-1}\hat{q}))|_k,\quad \Delta\hat{q}^{(m)}=\hat{q}^{(m+1)}-\hat{q}^{(m)} \tag{13}$$

and m is the pseudo-time iteration counter. Note, the coupling terms have been neglected in the left-hand side and therefore it depends directly only on the time-mean solution $\hat{q}_0^{(m)}$. As such the residual Jacobian $\frac{\partial R}{\partial q}$ is identical to that employed in the steady or unsteady nonlinear flow solver. The linear system of equations, Eqn. 12, is solved using either the incomplete lower upper (ILU) or successive overrelaxation (SSOR) methods.

3 VALIDATION

To quantify the errors induced by the adopted approximation of the Geometric Conservation Law (GCL) the impact of time-dependent mesh deformation on a uniform subsonic flow in a three-dimensional channel is investigated. The computation mesh and domain used in this work are shown in Fig. 1. The channel has a radial height of $\Delta r = 0.1$ m, a pitch $\Delta\phi = \frac{2\pi}{64}$, an outer radius $r_o = 1$ m and an axial length $l_x = 1$ m. The computational domain, with a total of 2×10^4 cells, is resolved with 200, 20 and 5 cells in the axial, radial and circumferential directions, respectively. In simulating the problem the nonlinear Euler equations are solved and a slip boundary condition is applied along all solid wall boundaries. At the inflow boundary the flow is purely axial with the uniform values of stagnation pressure and temperature of 101325 Pa and 288.15 K, respectively. At the outflow boundary a uniform value of static pressure of 85400 Pa is prescribed to give a flow with Mach number $M = 0.5$.

Time-dependent mesh motion is induced by prescribing axial displacement vectors on the inner and outer radial boundaries. The displacement vectors are given by

$$\tilde{x}=\begin{cases}\frac{\alpha}{2}\left(1+\cos\left(\frac{\pi(x-x_0)}{\Delta}\right)\right), & \text{if } |x-x_0|\le\Delta,\\ 0, & \text{otherwise,}\end{cases} \tag{14}$$

where Δ is the axial width of the disturbance, x_0 is its center and $\alpha \in [1, 0.5, 0.1]$ is the disturbance amplitude. The three-dimensional grid deformation is then computed using an elliptic mesh deformation algorithm [10]. The resulting distribution of the relative volume change ($\Delta V/V$) is shown in Fig. 1 for the amplitude $\alpha = 1$. It can be seen that this corresponds to a maximum relative volume change of approximately 30%. As a disturbance vectors prescribed on the inner and outer radial boundaries have only components in the axial direction the relative volume change varies linearly with the amplitude of the disturbance vectors. E.g. for $\alpha = 0.5$ and $\alpha = 0.1$ the maximum relative volume changes are approaximately 15% and 3%, respectively.

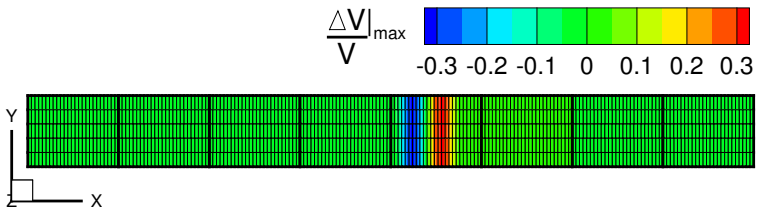

Figure 1: Channel Flow: Computation domain, topology, mesh and cell deformation.

The impact of mesh deformation on solution accuracy is shown in Fig. 2. Error is measured in terms of the maximum amplitude of the spurious pressure fluctuations ($|\Delta p|_{max}$). Ideally, the time-depedent mesh motion should produce no changes in the solution field. However, as the implemented approach only satisfies the GCL approximately, some influence on the solution quality is to be expected. In Fig. 2 the influence of displacement amplitude and frequency, between 10 Hz and 10000 Hz, is shown. It can be seen that the error varies approximately linearly with both disturbance frequency and displacement amplitude. Using the linear approximation to evaluate the time derivative of the Jacobain according to Eqn. 11 large spurious pressure fluctuations are obtained. When using the HB approach the spurious fluctuations are reduced by up to two orders of magnitude. For this approach, at the largest investigated frequency ($f = 10000$ Hz) and the largest relative volume change of 30% spurious pressure fluctions with amplitudes of approximately 50 Pa are observed. At more moderate frequencies and amplitudes the amplitude of the suprious pressure fluctuations is of the order 1 Pa. This emphasises that the HB formulation has to be used in the Harmonic Balance method to avoid the corruption of the results by spurious perturbations.

4 APPLICATION

To validate the HB-solver for flutter problems the extended solver is applied in this section to compute the well documented aeroelastic testcase Standard Configuration 10 (STCF10) [3]. STCF10 is a two-dimensional compressor cascade. The profile is constructed by superimposing the thickness distribution of a modified NACA0006 airfoil onto a circular-arc camber line. The stagger angle is 45 and the pitch to chord ratio is 1. The computational domain and mesh topology used in the simulations are shown in Fig. 3. The two-dimensional computational domain comprises a total of 5600 cells distributed over 6 blocks. The entry and exit boundaries of the computational domain are located approximately one chord length upstream and downstream of the compressor blade, respectively. In accordance with most data in the literature the test case is simulated by solving the nonlinear Euler equations.

To investigate the accuracy of the HB-solver STCF10 is simulated at two flow conditions: subsonic flow ($M_1 = 0.7$ and $\beta_1 = 55°$), and transonic flow ($M_1 = 0.8$ and $\beta_1 = 58°$). Figures 4 and 5 show the computed time-mean flow fields in terms of the isentropic Mach number M_{is}. At both operating points the numerical results agree very

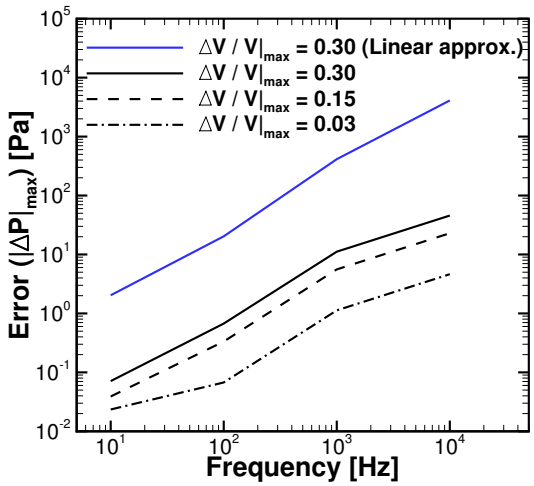

Figure 2: Channel Flow: Variation of error (in terms of pressure disturbance amplitude) with disturbance frequency and relative cell volume change.

well with the corresponding data from the literature [9]. The aeroelastic stability of the two-dimensional compressor cascade is investigated for a torsional mode with reduced frequency $\omega^* = c\omega/2|U|_{\text{Inlet}} = 0.5$, amplitude 0.1° and axis of rotation located at midchord. The computed values of aerodynamic damping, normalized against the value computed at $\sigma = 180°$, are shown in Fig. 7 and compared against reference data from the literature [9]. The HB simlations have been performed here using a single harmonic at the frequency of the eigenmode. As can be seen the HB solutions show excellent agreement with the linearTRACE results and the data from the literature, with the acoustic resonances at approximately $\sigma = -120°$ and $\sigma = -60°$ being well predicted. A comparison of the computed pressure disturbance fields is presented in Fig. 6. Here the real part of the complex valued pressure field at the first harmonic of the eigenmode is plotted for the interblade phase angle $\sigma = -130°$. Again the results show excellent agreement and demonstrate that the pseudo-time formulation of the nonreflecting boundary conditions used in the HB-solver perform equal well as their GMRES counterpart used in linearTRACE.

Under the subsonic flow conditions the computed values of aerodynamic damping were found to be largely insensitive to the amplitude of the torsional motion. In contrast, at the transonic flow condition the presence of the shock on the suction side of the compressor blade made the HB results very sensitive to the amplitude of the torsional motion. With an amplitude of 0.1° significant discrepencies (of the order 25%) were observed in the computed values of aerodynamic damping at interblade phase angles near ±180°. By reducing the amplitude of the torsional motion by an order of magnitude the results shown in Fig. 8 could be obtained. As can be seen the degree of agreement between linearTRACE and the HB-solver is for this amplitude excellent. Furthermore, good agreement is observed

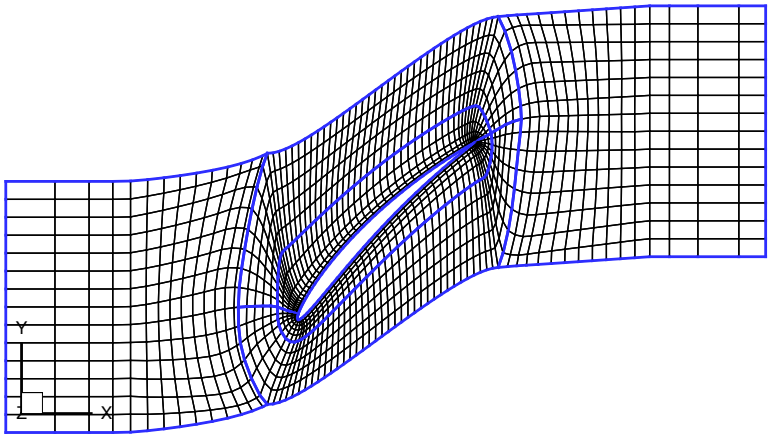

Figure 3: Standard Configuration 10: Computational domain, topology and mesh (every second mesh point only).

between the HB results and the data from the literature.

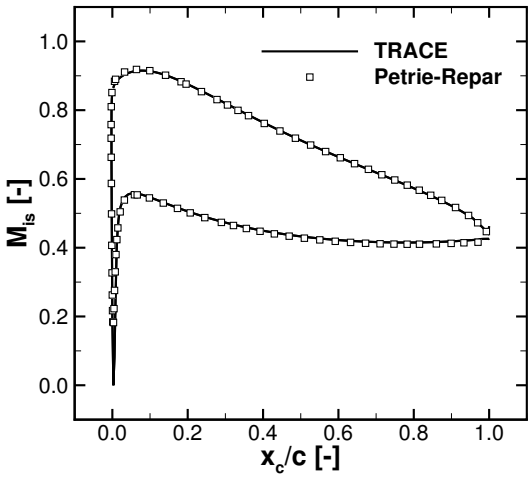

Figure 4: Standard Configuration 10: Comparison of isentropic Mach number distributions at subsonic flow conditions.

5 CONCLUSIONS

A Harmonic Balance solver has been extened and validated for the simulation of aeroelastic problems in the field of turbomachinery. The HB-algorithm and its extension for deforming meshes has been described in detail. Using a simple channel flow the impact of time-dependent mesh deformation on the accuracy of numerical method has been quanti-

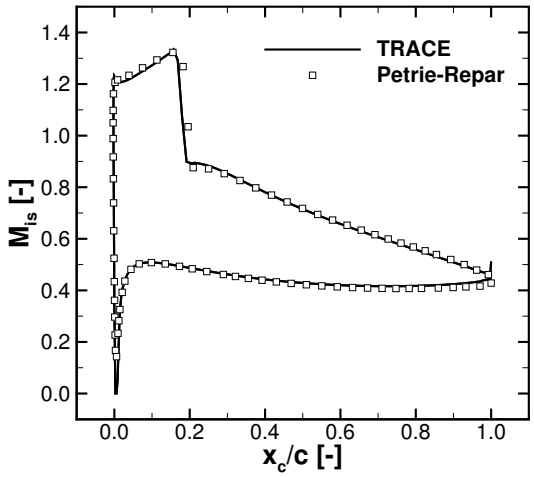

Figure 5: Standard Configuration 10: Comparison of isentropic Mach number distributions at transonic flow conditions.

fied. Results show that although time-dependent mesh deformation causes the generation of spurious pressure fluctuations, their amplitudes are only a small fraction of the amplitudes of typical physical pressure fluctuation induced for example by blade vibrations are therefore can be neglected in practical applications. Application of the HB-solver to the reference testcase Standard Configuration 10 has shown that the method can be used to accurately predict the flutter characteristics of the two-dimensional compressor cascade at both subsonic and transonic flow conditions. At transonic flow conditions numerical investigations indicate the presence of nonlinear flow effects for amplitudes of oscillation greater than 0.01°.

ACKNOWLEDGEMENTS

This work was supported by the German Federal Ministry of Economics and Technology under grant number 20T1104B.

REFERENCES

[1] K. Becker, K. Heitkamp, and E. Kügeler. Recent progress in a hybrid-grid CFD solver for turbomachinery flows. In *Proceedings Fifth European Conference on Computational Fluid Dynamics ECCOMAS CFD 2010*, 2010.

[2] M. Franke, T. Röber, E. Kügeler, and G. Ashcroft. Turbulence treatment in steady and unsteady turbomachinery flows. In *Proceedings Fifth European Conference on Computational Fluid Dynamics ECCOMAS CFD 2010*, Lisbon, Portugal, June 2010.

[3] T. H. Fransson and J. M. Verdon. Updated report on Standard Configurations for

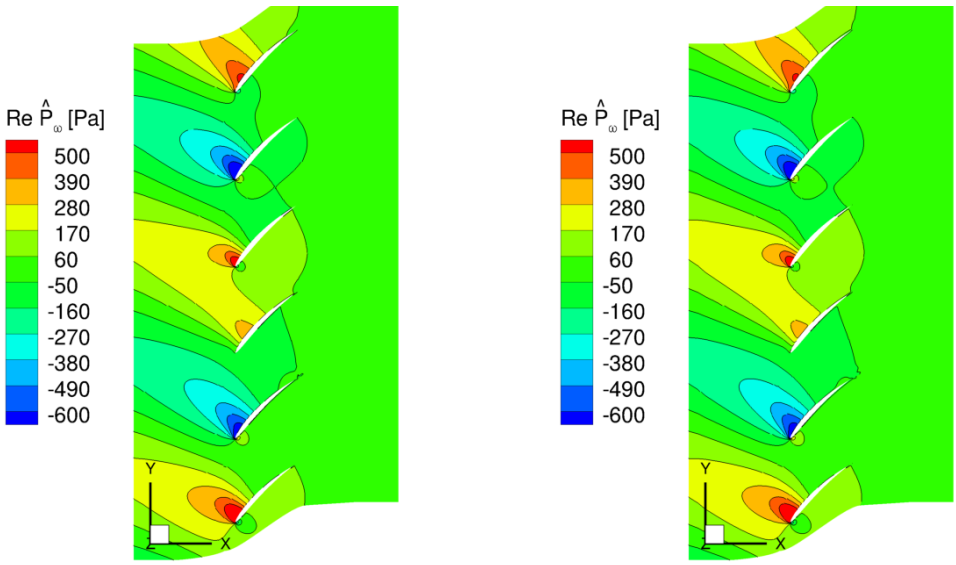

Figure 6: Comparison of the real parts of the computed pressure perturbation fields for Standard Configuration 10 with an inter-blade phase angle of -130 deg.: time-linearized method (left) and harmonic balance method (right).

the Determination of unsteady Flow Through Vibrating Axial-flow Turbomachine-Cascades. Technical Report TRITA/KRV/92.009, KTH, Stockholm, 1992.

[4] C. Frey, G. Ashcroft, H.-P. Kersken, and C. Voigt. A Harmonic Balance Technique for Multistage Turbomachinery Applications. In *Proceedings of the ASME Turbo Expo 2014*, 2014.

[5] M. B. Giles. Nonreflecting boundary conditions for Euler calculations. *AIAA Journal*, 28(12):2050–2058, 1990.

[6] T. Guedeney, A. Gomar, F. Gallard, F. Sicot, G. Dufour, and G. Puigt. Non-uniform time sampling for multiple-frequency harmonic balance computations. *Journal of Computational Physics*, 236:317–345, 2013.

[7] K. C. Hall and W. S. Clark. Linearized Euler predictions of unsteady aerodynamic loads in cascades. *AIAA Journal*, 31(3):540–550, 1993.

[8] H.-P. Kersken, C. Frey, C. Voigt, and G. Ashcroft. Time-Linearized and Time-Accurate 3D RANS Methods for Aeroelastic Analysis in Turbomachinery. *J. Turbomach.*, 134(5), 2012.

[9] P. J. Petrie-Repar, A. McGhee, and P. A. Jacobs. Three-Dimensional Viscous Flutter Analysis of Standard Configuration 10. *ASME Paper No. GT2007-27800*, 2007.

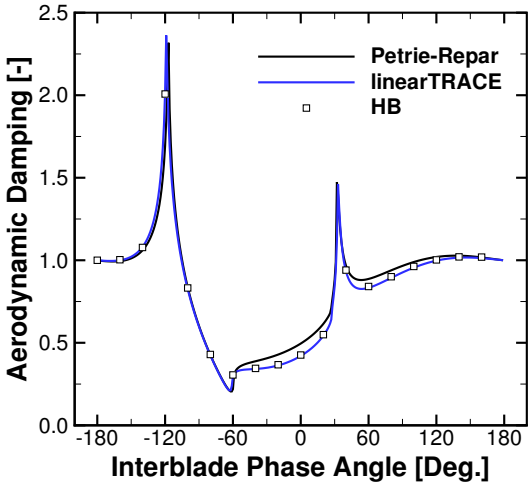

Figure 7: Normalized Aerodynamic Damping at Subsonic Flow Conditions and $\omega^* = 0.5$.

[10] C. Voigt, C. Frey, and H.-P. Kersken. Development of a generic surface mapping algorithm for fluid-structure-interaction simulations in turbomachinery. In J. C. F. Pereira, A. Sequeira, and J. M. C. Pereira, editors, *V European Conference on Computational Fluid Dynamics ECCOMAS CFD 2010*, June 2010.

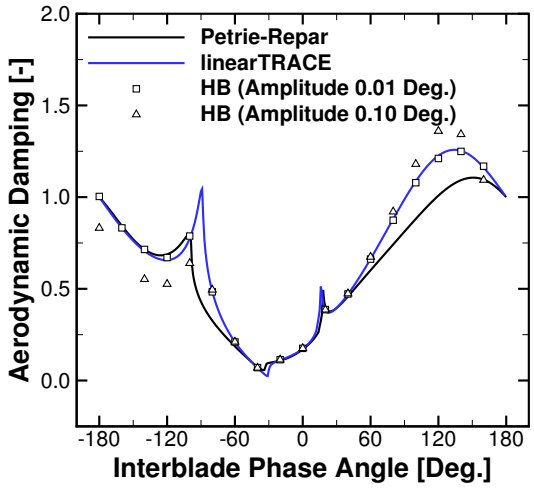

Figure 8: Normalized Aerodynamic Damping at Transonic Flow Conditions and $\omega^* = 0.25$.